PCCP

Physical Chemistry Chemical Physics

www.rsc.org/pccp

Volume 15 | Number 7 | 21 February 2013 | Pages 2233–2604

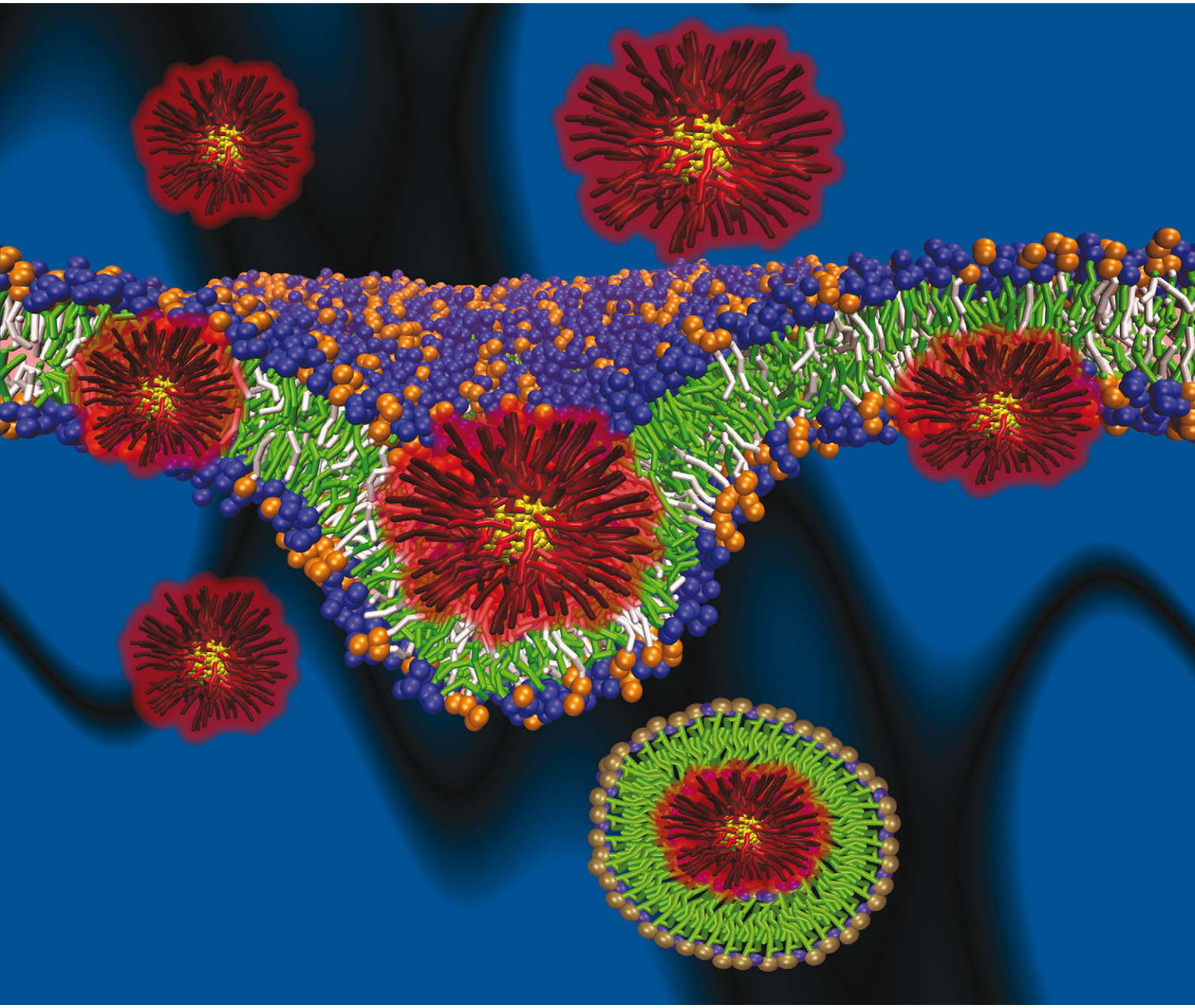

ISSN 1463-9076

PAPER

da Rocha *et al*.

Nanoparticle translocation through a lipid bilayer tuned by surface chemistry

1463-9076(2013)15:7;1-F

PCCP

RSC Publishing

PAPER

View Article Online
View Journal | View Issue

Cite this: *Phys. Chem. Chem. Phys.*, 2013, **15**, 2282

Nanoparticle translocation through a lipid bilayer tuned by surface chemistry†

Edroaldo Lummertz da Rocha,*[a] Giovanni Finoto Caramori[b] and Carlos Renato Rambo[a]

Received 21st September 2012,
Accepted 16th November 2012

DOI: 10.1039/c2cp44035k

www.rsc.org/pccp

An enhanced understanding about the interactions between nanomaterials and cell membranes may have important implications for biomedical applications. In this work, coarse-grained molecular dynamics simulations of gold nanoparticles interacting with lipid bilayers were performed to evaluate the effect of hydrophobicity, charge density and ligand length on lipid bilayers. The simulations accomplished indicate that hydrophobic and anionic nanoparticles do not exhibit significant interactions and different charge densities may induce pore formation or nanoparticle wrapping, resembling first stages of endocytosis. The suggested interplay between charge density and ligand length has important implications when designing nanoparticles for drug and gene delivery applications. Moreover, control of charge densities may induce internalization of nanoparticles into cells through different mechanisms such as passive translocation, for nanoparticles with low charge density, or endocytosis for higher charge densities, highlighting the role of surface chemistry in nanoparticle–cell interactions.

1 Introduction

Nanomaterials are promising platforms for theragnostic applications.[1] Their multifunctional properties such as drug encapsulation, tumor targeting and photothermal therapy can be explored for drug and gene delivery in cancer treatment[2] and regenerative medicine.[3,4] The comprehension about the interactions between nanomaterials and biological systems (in particular cell membranes) is crucial to move nanotechnology towards biomedical applications.[5] Several theoretical and experimental investigations indicate that the physicochemical properties of nanoparticles such as size, morphology and surface chemistry define the biodistribution profiles,[6] absorption by cells[5,7] and toxicity of these nanoscale materials.

Nanoparticles have to overcome several biological barriers to achieve tumor targeting, drug delivery and photothermal or photodynamic therapy.[8,9] In the circulatory system these materials have to escape from elimination by the organism defenses, avoid nonspecific binding with serum proteins, target cancer cells or tumor vasculature,[10] diffuse into tumor microenvironments,[11] penetrate cell membranes and, in some cases, also diffuse through the nuclear membrane. Employing the knowledge of tumor biology with the design of nanoparticles may lead to more effective delivery systems, reducing off-target effects and enhancing the treatments.[1]

However, due to the multiscale nature of targeting and delivering payloads to cells, different approaches are being employed.[2,12–19] Nanoscale interactions are particularly interesting since physicochemical aspects of nanoparticles affect their interaction with cells in a great extension *in vitro* and also *in vivo*.[20] These interactions can be evaluated using coarse-grained molecular dynamics (CGMD) simulations as indicated by several recent investigations.[13,21] Experimental and computer simulations were performed by Shi and colleagues[22] to understand the cell-entry mechanisms of one-dimensional nanomaterials. The authors showed that the internalization process is dependent on adenosine triphosphate (ATP) and the tip entry is the predominant uptake behavior as indicated by dissipative particle dynamics (DPD). Yang and Ma have shown that the shape anisotropy and orientation of the nanoparticle affect significantly the interaction with a coarse-grained lipid bilayer model and rotation movements confer additional obstacles to the translocation process.[16] Recent investigations use the MARTINI forcefield to create lipid bilayer models and study the effect of nanoparticles on structural properties of membranes such as

[a] *Graduate Program in Materials Science and Engineering, Federal University of Santa Catarina, Florianpolis, SC, Brazil. E-mail: edroaldo@gmail.com*
[b] *Chemistry Department, Federal University of Santa Catarina, Florianpolis, SC, Brazil*

† Electronic supplementary information (ESI) available: Snapshots of simulations of nanoparticles with 15 and 25% of charge, density profiles for the cases with 40, 60 and 80% of charge and simulations performed using larger membranes (40 × 40 nm) with 20 and 100% of charge are provided. See DOI: 10.1039/c2cp44035k

charge density, size and conditions to hole formation on the membrane surface.[15,23,24] Examples of nanomaterials investigated using this simulation approach include dendrimers, fullerenes, carbon nanotubes and gold nanoparticles.[23,25–31]

Molecular modeling approaches have shown to be a valuable tool not only for designing nanoparticles, including size, shape and surface chemistry, but also for describing dynamical interactions[12,16,25,32] involving the nano–bio interface,[20] providing qualitative results in good agreement with experimental ones.[5,7,22,33] It is highly desirable to create predictive tools for evaluating nanomaterials prior to experimentation since this may reduce costs, and raise the chances of success *in vivo*. Although the majority of the current computational investigations are concerned about the impact of size and shape of nanomaterials on cell internalization, just a few ones investigate the importance of surface chemistry for these processes. However, experimentally, the surface chemistry of nanoparticles has a profound impact on how nanoparticles penetrate cell membranes.[5,7] Exploring the functionalization of nanoparticles with high affinity moieties to the cell surface, receptor-mediated endocytosis may be favored. In addition, passive internalization processes may be promoted with a smart surface chemistry design. As cancer cell membranes are slightly negative, cationic nanoparticles are capable of penetrating cell membranes more efficiently compared to neutral and anionic counterparts and the functionalization with cell-penetrating peptides (CPPs) and, importantly, synthetic ligands inspired by natural CPPs design, effectively are able to passively cross cell membranes.[7] In this work, systematic investigations at the molecular level are accomplished in order to understand the influence of charge density and the length of the ligand on internalization of nanoparticles by cells. This investigation might not only provide a better comprehension of the role of ligands (such as charged ligands with different lengths) in cell interactions but might also be a valuable tool for designing nanoparticle–cell interactions.

2 Methodology

2.1 Nanoparticle and membrane coarse-graining

Atomistic molecular dynamics simulations were performed to build a self-assembled monolayer (SAM) of alkyl thiol ligands over the gold nanoparticle surface. The core of the nanoparticles investigated is characterized by a face-centered cubic (FCC) lattice, truncated-octahedron (TO) structure and a diameter of 2.2 nm. The TO core was obtained by cutting a bulk FCC lattice and the Packmol[34] software was used to insert 100 alkyl thiol molecules in a sphere close to the surface of the gold core. The LAMMPS[35] software was employed to build the atomistic models.

The gold core was equilibrated at room temperature applying the embedded-atom method (EAM)[36] as a many-body potential and several combined forcefields were employed to form a SAM on the surface of the nanoparticle. A united-atom potential was used to describe intra- and inter-molecular interactions of alkyl segments, whilst the Morse potential for gold–sulfur interactions and the Lennard-Jones potential for sulfur–sulfur and sulfur–alkyl interactions were employed. A cycled annealing procedure was accomplished to form the self-assembled monolayer of ligands on the gold surface. Therefore, after the atomistic simulations, a gold nanocluster passivated with SAMs was then obtained. Charges were added to terminal sites of the ligands and randomly distributed throughout the nanoparticle.

The MARTINI forcefield for biomolecular simulations[37,38] was used to coarse-grain the systems. This forcefield was extensively validated to simulate the self-assembling in lipid systems including vesicles,[39,40] liposomes[41] and lipid bilayers.[37,38] In this forcefield every four heavy atoms (not hydrogen) are mapped to one effective bead reducing the computational efforts. Different levels of interaction are represented by four primary types of beads, polar (P), apolar (C), nonpolar (N) and charged (Q). Several subtypes are defined within each principal type of bead to describe more appropriately the chemical nature of the represented atoms in terms of the hydrogen-bonding capability and different levels of polarity.[38]

Considering these types of beads and the subjacent chemical nature of the nanoparticles, the coarse-graining of these structures was performed mapping gold and sulfur atoms 1 : 1 into coarse-grained beads that were rigidly fixed in the new coarse-grained model. The alkyl chains were 4 : 1 mapped and assigned interaction sites C1 in MARTINI. These coarse-grained beads were connected by harmonic bonds and restrained by harmonic angles as defined in the MARTINI forcefield.

Two biomembrane models were employed. The first one is characterized by neutral net charge and it is composed of dipalmitoylphosphatidylcholine (DPPC) lipids. The Packmol software was used to build the lipid bilayers from only one coarse-grained DPPC lipid model. The second lipid bilayer is a mixture of DPPC and dipalmitoylphosphatidylglycerol (DPPG) lipids. Both coarse-grained lipid models contain 12 beads but DPPG has a glycerol group instead of a choline group, which confers a negative net charge to lipid. The negative lipid bilayer is constructed from the neutral bilayer replacing randomly DPPC molecules for DPPG lipids in a ratio of 3 : 1. The parameters of DPPC and DPPG are those defined in the MARTINI force field.

Each lipid bilayer system was inserted in a cubic simulation box and immersed in water. The dimensions of the box are 20 × 20 × 20 nm. The lipid bilayers considered are composed of 1200 lipids and water beads were added to fill the simulation box. Firstly, the system water–bilayer was equilibrated using the isothermal–isobaric ensemble (NPT ensemble). After equilibration, the nanoparticle was placed at 6 nm above the bilayer center. The distance of 6 nm was chosen especially due to the box dimensions 20 × 20 × 20 nm, in which the membrane is placed about 5 nm below the center of the box. Therefore, the distance of the nanoparticle from the membrane surface to the maximum height of the box is approximately 15 nm. Thus, the nanoparticle containing the ligands (approx. 4 nm diameter) was placed at the half of this distance, avoiding direct contact between the nanoparticle and ensuring that the whole particle is in the simulation box. Na^+ and Cl^- ions were added to neutralize the system and periodic boundary conditions were applied. The simulations were performed using integration time steps of 20 fs. Temperature was set to 305 K using the

Berendsen thermostat,[42] pressure coupling was applied to maintain the pressure at 1 bar using the Berendsen barostat.[42] The cutoff of short-ranged Coulombic interactions and van der Waals interactions was 1.2 nm. The mesh Ewald summation (PME) method[43] was used to describe long-range Coulombic interactions. The coarse-grained simulations were executed with the GROMACS 4.5.3 software.[44] All simulations were performed at least twice to ensure reproducibility of the results.

3 Results and discussion

Fig. 1 illustrates the simulations for six different configurations of the nanoparticle–lipid bilayer system after 50 ns. These systems are constituted by two lipid bilayers (DPPC and DPPC/DPPG) and three different nanoparticles (cationic, anionic and hydrophobic). Considering these simulation snapshots, clear favorable interactions between the gold nanoparticle and the lipid bilayer are observed in cases (a), (b) and (f), where the nanoparticle was adsorbed on the surface of the membrane after 50 ns unbiased simulations. Systems (b) and (f) are consistent with dendrimer–membrane simulations.[12] However, due to electrostatic interactions between the cationic nanoparticle and the anionic biomembrane, the snapshot in case (a) exhibits a tendency to nanoparticle wrapping.

In cases (c), (d) and (e) nanoparticle–membrane interactions are not spontaneously favored. The lack of spontaneity might be associated with electrostatic interactions between both anionic components in this system. However, *in vivo*, anionic nanoparticles penetrate cell membranes although in a lesser extension compared to cationic nanoparticles. In our simulations, nevertheless, anionic nanoparticles are not adsorbed on nanoparticle's surface. Therefore, small energy barriers may exist between the nanoparticle and the lipid bilayer and avoid the adsorption and internalization processes. Therefore, an external force may be necessary to cause these phenomena in computer simulations. From the simulations, the chemical nature of nanoparticles may affect the interaction with lipid bilayers. As expected, cationic nanoparticles interact preferably with anionic biomembranes. Hence, as the cell membrane of cancer cells is slightly negative,[23] this surface chemistry can increase cell internalization efficacy. However, penetration of nanoparticles was not observed during simulation periods evaluated here and these behaviors have been achievable up to date only with a higher level of coarse-graining.[16,45]

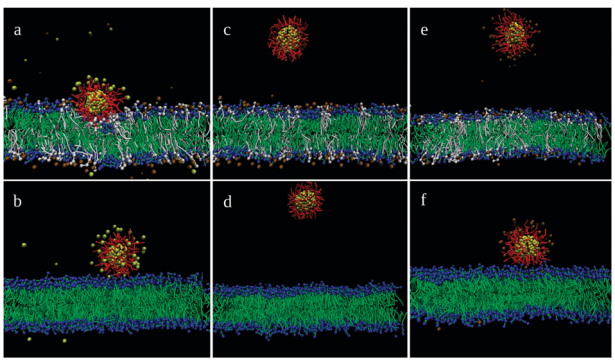

Fig. 1 Interactions of gold nanoparticles with different surface chemistries and two kinds of lipid bilayers. Lipid bilayers in the pictures (a), (c) and (e) are anionic (DPPC/DPPG lipids) and are interacting with cationic, hydrophobic and anionic nanoparticles, respectively. In pictures (b), (d) and (f), these nanoparticles are interacting with the neutral (DPPC) lipid bilayer. Colors: DPPC headgroups are shown in blue with tails in green. DPPG lipids, both headgroups and tails, are in white. The nanoparticle cores are in yellow and ligands in red. Ions Na^+ and Cl^- are in ochre and yellow, respectively.

Despite the complexity of biological cell membranes related to lipid heterogeneity, high density of membrane proteins and highly dynamical behavior associate with the cell microenvironment, the tendencies presented are consistent with previous simulations and experimental research.[23,24,33,46,47] Furthermore, it suggests that this nanoscale interface might be qualitatively approached using molecular modeling techniques, especially employing multiscale simulations. Based on the discussion above, it was observed that cationic nanoparticles favorably adsorbed on the cell membrane. Therefore, the role of charge density followed by ligand length in nanoparticle–membrane interactions is investigated in the following sections.

3.1 Effect of surface charge density

The effect of surface charge density on nanoparticle–membrane interactions was investigated by building six systems consisting of a nanoparticle with 0, 20, 40, 60, 80 and 100% of cationic coating interacting with a negative lipid bilayer. The surface charge affects the nanoparticle interaction through different mechanisms. Fig. 2 illustrates snapshots after 100 ns simulations. Interestingly, 20% charge density favored the nanoparticle penetration through the membrane upper leaflet and remains stable inside the hydrophobic region of the bilayer during the simulation time. In agreement with previous simulations with dendrimers[12,21] in biomembranes, a nanoscale pore was formed which indicates disruption of membrane lower and upper leaflets. These results also are in agreement with dendrimer simulations accomplished by Ainalem and colleagues[26] where dendrimers were able to penetrate into the hydrophobic region of the bilayer, adopting a transmembrane configuration with charged atoms interacting with lipid headgroups and the core of the dendrimer remained stable inside the hydrophobic region of the membrane, similar to nanoparticles simulated here. For density profiles of these systems, see the ESI† (Fig. S2 and S3).

Considering the simulation trajectories for nanoparticles with 20, 40, 60 and 80% of charge, an interplay between charge density and counterion interactions was observed, which probably explains these phenomena. For 20% of charge, in the beginning of the simulations, just few counterions interact with the cationic terminals of the nanoparticle. As the simulation proceeds, cationic terminals start to interact with phosphate groups in the opposite side of the membrane. When it happens, the nanoparticle penetrates into the lipid bilayer and remains in the hydrophobic core of the membrane. Therefore, interactions between cationic terminals of the nanoparticle and charged lipid headgroups as well as the hydrophobic nature of the gold core create a stable configuration that probably makes the complete translocation of the nanoparticle difficult. For 40, 60 and 80% of charge, more counterions around the nanoparticle were

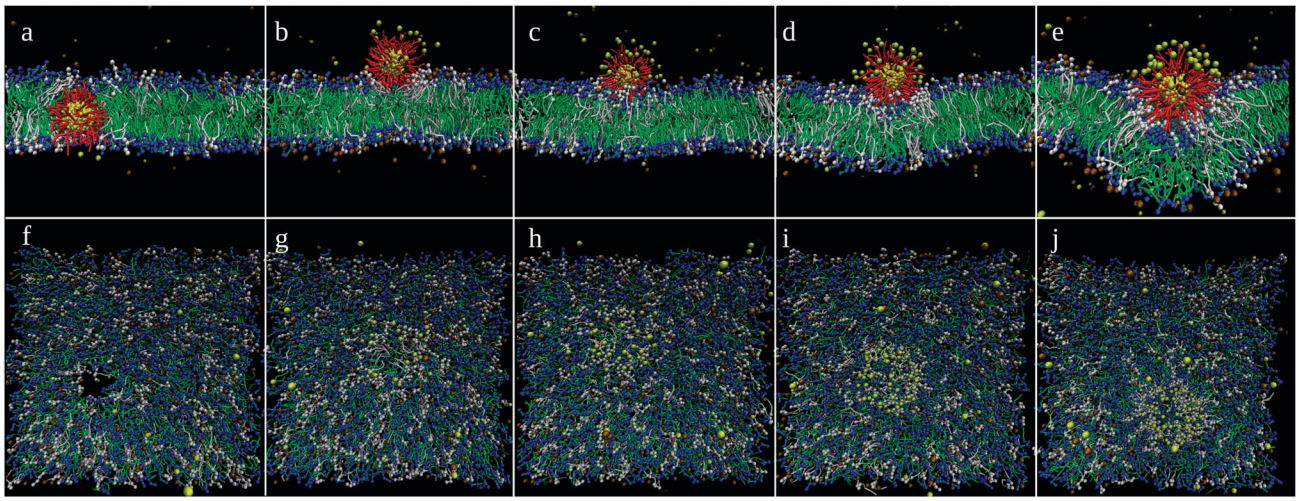

Fig. 2 Interactions of gold nanoparticles with different cationic coatings and negative lipid bilayers. (a), (b), (c), (d) and (e) display cross-section views of the nanoparticle–membrane systems with 20, 40, 60, 80 and 100% of charge density, respectively. (f), (g), (h), (i) and (j) display top views of these systems.

observed during the entire simulation time that avoid stronger interactions with phosphate groups in both leaflets of the membrane, which act as a barrier for translocation. However, it should be pointed out that the charge density is not high enough to induce wrapping of the nanoparticle, which is the case for 100% of charge.

In addition, it was previously demonstrated that Janus nanoparticles present two different interaction modes that are associated with their hydrophobic/hydrophilic nature, where nanoparticles are able to insert into the membrane or are engulfed by the lipid bilayer.[48] In the simulations presented here, when low charge densities are used, the hydrophobic property of the nanoparticles is more prominent than the charge. In this case, the charge is enough to mediate the attraction of the nanoparticle towards the membrane and hydrophobic interactions induce nanoparticle penetration. However, as the charge density raises, the nanoparticle exhibits a more hydrophilic nature and interactions with the negative phosphate groups from the lipid bilayer cause the attachment of the nanoparticle, starting a wrapping process similar to that observed for Janus nanoparticles.[48]

Despite the selective (macro)molecules transport properties of cell membranes in which small molecules such as O_2 and CO_2 are able to diffuse passively into cells, cell membranes employ different mechanisms to transport important ions and nanoscale proteins through specialized membrane transport proteins. Interestingly, nanomaterials may be designed to translocate passively[5] through cell membranes and transient pores formation might be a plausible mechanism such as that suggested by internalization of cell-penetrating peptides[49] besides related studies based on dendrimers.[12,25,26]

Raising the charge density to 40%, the nanoparticle induced low disorder on its local neighborhood while nanoparticles with 60 and 80% of charge exhibited a slightly different behavior. For these charge densities, nanoparticles begin to experience wrapping by the bilayer. This is evident in the case where a 100% of charge is present. For high charge densities, the nanoparticles cause global changes in the membrane dynamics reducing its surface area to accommodate these particles. Using this process the integrity of the bilayer is preserved and the nanoparticle is not able to translocate into the hydrophobic region of the membrane.

Structural properties of these systems were calculated and plotted in Fig. 3. A relationship between defective areas and membrane shrinkage was observed. The defective areas were pronounced with nanoparticles with 20, 40 and 60% of charge (Fig. 3(a)). Interestingly, simulations revealed that the nanoparticle with 20% of charge more effectively penetrated into the lipid bilayer and disrupted the lower and upper leaflets. Simulations with 15 and 25% of charge (see Fig. S1, ESI†) are also performed and nanoparticle behavior was similar, generating a nanopore on the membrane surface (Fig. 2(a) and (f)). In addition, simulations using a 40 × 40 nm also were performed and results were similar (Fig. S4, ESI†). However, although the cases of 40 and 60% of charge induced lipid reorganization when the nanoparticle was adsorbed on the surface of the membrane, the extension of these disruptions occurs only on the upper leaflet and the defective areas induced by these charge densities are more than 50% lower compared to nanoparticles with 20% of charge.

As charge density increases the disrupted areas are reduced since the nanoparticle is adsorbed on the surface. However, instead of penetration the behavior observed was a tendency to nanoparticle wrapping as evidenced by membrane shrinkage, Fig. 3(b), and the reduction of disrupted areas. Therefore, the membrane integrity is preserved and the passive translocation is avoided. When 100% of charge is employed the membrane exhibited 14.25% reduction of its original surface area. This tendency to wrapping is observed in previous simulations employing dissipative particle dynamics (DPD).[45] The root mean square error (RMSD) was measured, Fig. 3(c), and its maximum value occurs for the nanoparticle with 20% of charge which indicates more significant structural deviations.

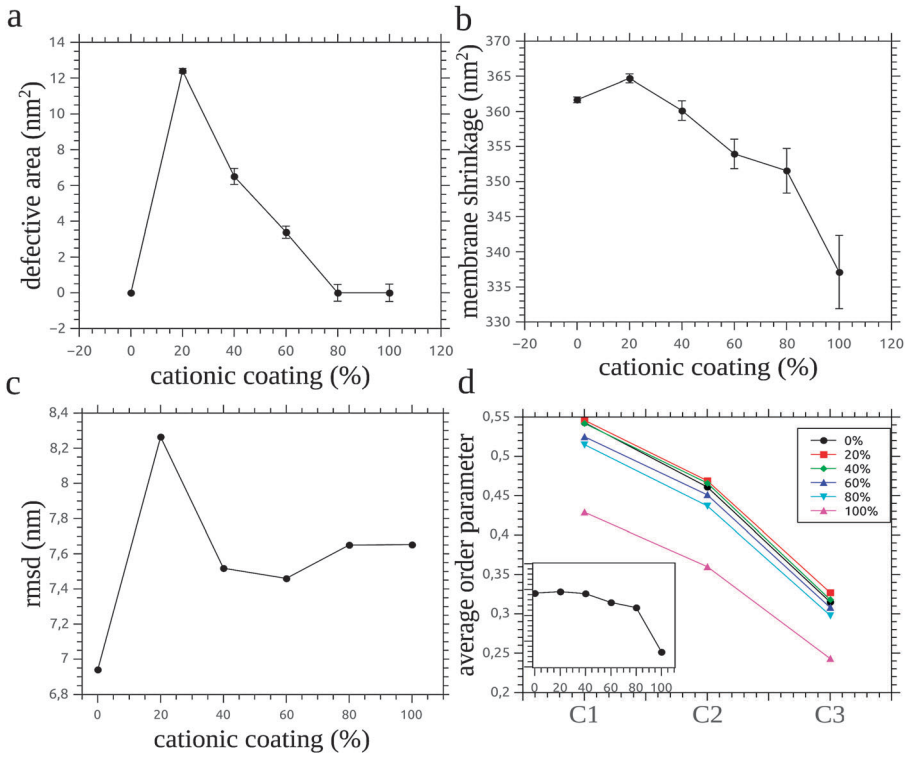

Fig. 3 Structural properties of the membranes as a function of charge density. (a) Defective areas induced by the nanoparticle with different surface charge density, (b) membrane shrinkage during adsorption and disruption/wrapping processes, (c) the root-mean-square deviation between the equilibrated membrane and the membrane interacting with the nanoparticle. (d) Lipid reorganization as measured by average order parameter.

The average order parameter was calculated to analyze the effect of charge on structural properties of the membrane, Fig. 3(d). Order parameters vary between 1 (perfect orientation in the bilayer normal) and −0.5 (anti-alignment) or 0 for random orientation. Comparing the case with 0 and 20% of charge, a slight raise in the order parameters is observed. Probably it happens due to the reduction of the surface area of the lipid bilayer when a nanopore is formed. These pores occupy 12.40 nm^2 of the membrane surface and may induce the reorganization of lipids towards a more ordered phase.

Here, the order parameters are related to nanoparticle wrapping since they are calculated based on the bilayer normal. As the surface charge increases the membrane surface area is reduced as observed in Fig. 2(e), (j) and 3(b). Therefore, the reduction of order parameters is consistent with membrane shrinkage and the tendency to engulf the nanoparticle, as evidenced by the nanoparticle with 100% of charge. Accordingly, order parameters in this analysis are related to membrane curvatures not membrane disruptions. The inset in Fig. 3(d) displays the order parameters for C1–C2 bonds in the lipid molecule, emphasizing the wrapping behavior. Similar curves are obtained for C2–C3 and C3–C4 bonds in the lipid tails.

Radial distribution functions (RDFs) of DPPC, DPPG and water around the nanoparticle are illustrated in Fig. 4(a) and (b). For 20% of charge, Fig. 4(a), the behavior of DPPC and DPPG around the nanoparticle is similar. However, DPPG lipids are closer to the nanoparticle surface due to favorable electrostatic interactions. The sharp peak at 0.25 nm is observed for DPPG lipids emphasizing the importance of charge complementarity for these interactions. However, due to the pore formation, both DPPG and DPPC lipids are around the nanoparticle.

Fig. 4(b) shows the RDF of the nanoparticle with 100% of charge. The peak intensity for DPPG lipids close to 0.25 nm is considerably higher than that for DPPC lipids and much more DPPG lipids are around the nanoparticle. In both cases, 20 and 100% of charge, these RDF curves show that positively charged terminals interact more strongly with lipids with negative overall charge although these interactions also occur for negative head groups from DPPC lipids. These results suggest that electrostatic interactions are important for penetration or wrapping of nanoparticles into or by lipid bilayers and may induce pore formation or the first stages of endocytosis, respectively.

3.2 Effect of ligand length

The effect of ligand length also was investigated using coarse-grained molecular dynamics simulations. Three ligands were considered: 1-octanethiol, 1-dodecanethiol and 1-hexadecanethiol. Simulations of these systems with 20 and 100% of charge were performed and the results suggest an interesting interplay between charge density and ligand length. Fig. 5(a)–(f) shows snapshots of the systems at the end of 100 ns of simulation.

The behavior associated with nanoparticles coated by 1-octanethiol with 20 and 100% of charge was described previously. Very different interactions are obtained when the ligand is 1-dodecanethiol or 1-hexadecanethiol and 20% of charge is employed, Fig. 5(b) and (c), compared to Fig. 5(a). In Fig. 5(g),

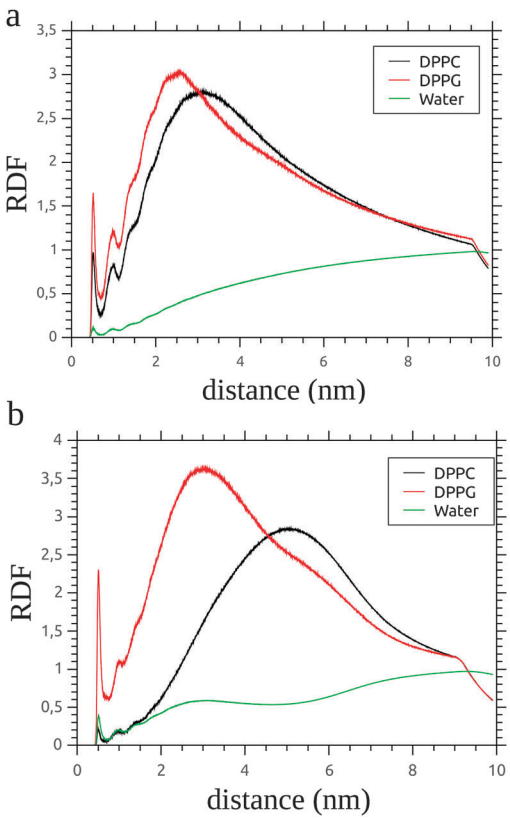

Fig. 4 Radial distribution functions between DPPC, DPPG, water and the cationic gold nanoparticle. (a) shows RDFs for nanoparticles with 20% of charge while (b) presents RDFs for nanoparticles with 100% of charge.

RDFs of 1-octanethiol terminals and phosphate groups of biomembrane are plotted for charges of 20 and 100%. Comparing the relative intensities of the peaks close to 0.25 nm, the electrostatic interactions are stronger for the nanoparticle with 100% of charge than the one with 20%, as expected. However, due to nanoparticle penetration, a peak is observed in both cases. Insets show RDF from nanoparticle's cationic terminals and positive choline groups of the bilayer. The relative intensities indicate that phosphate groups interact more strongly with cationic terminals of the nanoparticle than choline groups, suggesting that these electrostatic interactions are important to nanoparticle penetration or wrapping. A similar behavior is observed in Fig. 5(h) and (i).

Although phosphate groups interact similarly for nanoparticles with 20 and 100% of charge, a slightly different behavior is observed in the interaction between cationic terminals of the nanoparticle and counterions Cl^- added to provide electroneutrality to the system. Analyzing the RDFs in Fig. 6, the length of the ligand has an important role in the interaction with counterions when 20% of charge is employed, in which the peak intensity is significantly lower than RDF for the nanoparticle with 100% of charge, Fig. 6(a). Furthermore, despite the difference in the peak intensities of the nanoparticles with 20 and 100% of charge in Fig. 6(b) and(c), it is still less pronounced than the difference observed in Fig. 6(a).

The favorable penetration obtained for nanoparticles coated by 1-octanethiols and with 20% of charge may be related to weak electrostatic interactions existing between cationic terminals and counterions while keeping significant interactions with negative phosphate groups of the lipid bilayer, Fig. 5(g). Nanoparticles with 1-dodecanethiol and 1-hexadecanethiol did not exhibit a tendency to penetrate the membrane probably due to significant interactions with counterions as evidenced in Fig. 6(b) and (c) as weaker interactions with phosphate groups of the bilayer, Fig. 5(h) and (i). However, 100% of charge induces stronger electrostatic interactions leading to bilayer surface area reduction, restoration of the membrane thickness and wrapping of the nanoparticle. It is observed for all systems with 100% of charge although in a lower extension for the 1-hexadecanethiol ligand.

Nanoparticles coated by longer ligands exhibit a large effective radius, which promotes stronger interactions with counterions in solution and a reduction in the interaction strength with the lipid bilayer when low charge densities are employed. Although it is previously demonstrated that longer ligands are more effectively wrapped by a lipid bilayer using DPD,[50] the simulations in the present study show that it only happens when higher charge densities are employed, where nanoparticle–membrane interactions are strong. When low charge densities are used, longer ligands present neither nanoparticles translocation nor wrapping. Therefore, a large effective radius is not enough to induce nanoparticle wrapping. In light of this, in particles with large effective radius a higher number of counterions will most likely interact with the ligands, creating a shielding effect, avoiding nanoparticle penetration. Evaluating the simulation trajectories, it was observed that counterions exhibit weaker interactions with nanoparticles with short ligands compared to nanoparticles with long ligands before adsorption and penetration. These weak interactions remain after nanoparticle penetration for short ligands that induce translocation and they become more evident for long ligands that promote wrapping. Together these results suggest not only a plausible mechanism in which both charge density and ligand length affect nanoparticle–membrane interactions but also how they affect membrane dynamics and structure.

4 Modeling nanoparticle–membrane interactions

The interest of this research was to investigate how the surface chemistry may influence the internalization of nanoparticles into cells. Simulations with nanoparticles with low charge density presented a behavior consistent with dendrimer simulations,[12] where a nanosized hole was formed in the membrane. These results suggested a strategy to escape from endocytic pathways favoring the passive translocation through the lipid bilayer and inducing minimal membrane disruptions. Nanoparticles that penetrate cell membranes frequently are trapped inside lysosomes and these materials need some mechanism to promote lysosomal escape, which is crucial for many drug and gene delivery applications.

Moreover, nanoparticles with a low charge density present reduced toxicity and nonspecific binding occurs in a lesser

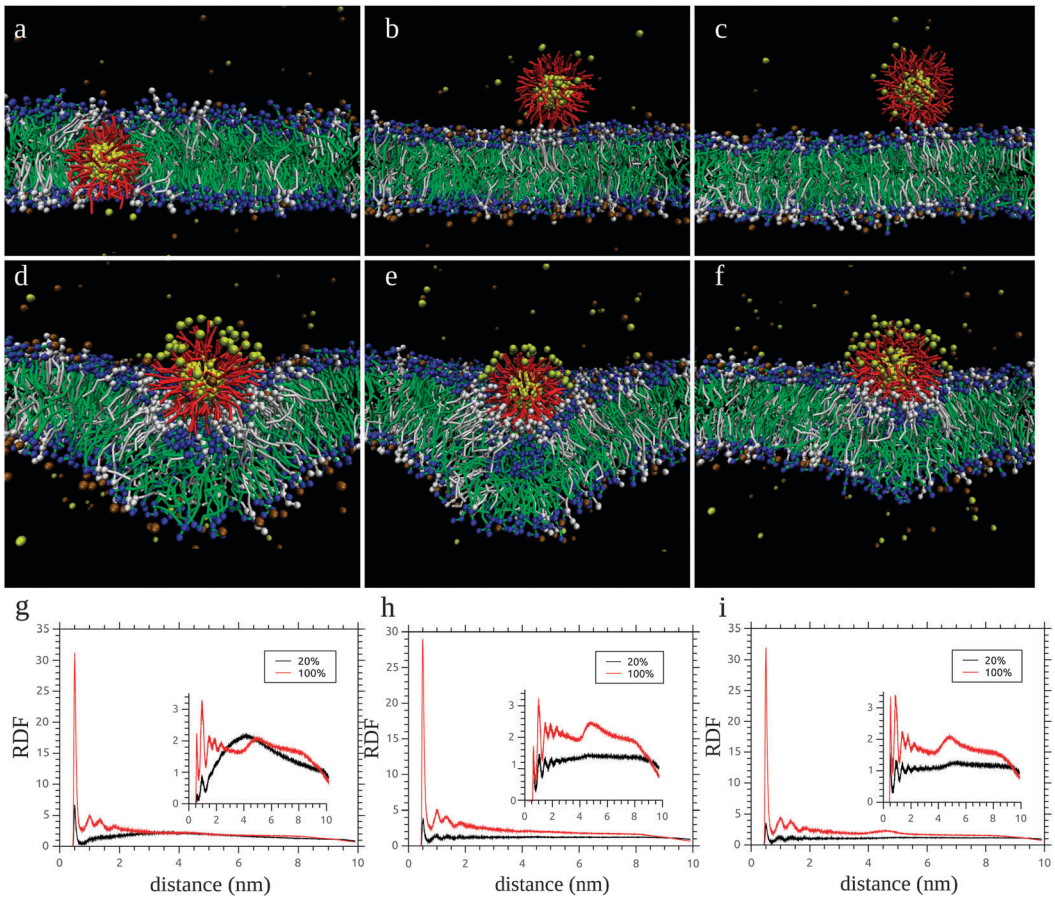

Fig. 5 Effect of ligand length and surface charge on nanoparticle–membrane interactions. (a), (b) and (c) illustrate nanoparticles with 20% of charge and the ligands 1-octanethiol, 1-dodecanethiol and 1-hexadecanethiol, respectively. (d), (e) and (f) display nanoparticles with 100% of charge and same ligands previously considered. (g), (h) and (i) are plots of the radial distribution functions between nanoparticle's cationic terminals and the negatively charged phosphate groups from the lipid bilayer. Insets present RDFs from nanoparticle's cationic terminals and positive choline groups of the bilayer.

extension than high charge density designs. In biomedical applications, a balance between internalization efficacy and toxicity needs to be considered. Therefore, nanoparticles with low content of charge would satisfy this requirement. However, our simulations suggest that ligands with different lengths affect significantly the penetration of nanoparticles. Although nanoparticles functionalized with 1-octanethiol and 20% of charge were able to penetrate the bilayer, for the same charge density, 1-dodecanethiol and 1-hexadecanethiol did not present such behavior. Therefore, nanoparticles functionalized with 1-octanethiol and low charge densities would favor the passive translocation through cell membranes avoiding the need to design lysosomal escape mechanisms.

On the other hand, intermediary charge densities did not present a behavior distinctive of adsorption on the membrane surface in our simulations. The observed tendency indicates that higher charge densities tend to induce nanoparticle wrapping. This behavior is consistent with previous simulations using dissipative particle dynamics[45] and resembles the initial processes associated with endocytosis, although membrane receptors are not employed here. For 100% of charge all ligands considered wrapped the nanoparticle although with 1-hexadecanethiol this effect was less significant.

In light of the presented results, nanoparticles with high charge density may be internalized by cells using an endocytic pathway more readily than low charge density ones. Although other studies suggest that high density charge nanoparticles are more disruptive, when a low concentration of nanoparticles is employed, nanoparticle engulfment may be actually favored and the disruptive regions would be reduced. Therefore, although in these cases nonspecific binding may be significant, smart surface chemistry may overcome this issue and expose the positive charges at the cancer cell–nanoparticle interface.[51] Internalization is then favored, reducing nonspecific binding and systemic toxicity.

The complexity of *in vivo* systems used to evaluate nano-based therapies is motivating convergence between several research areas. Using molecular simulations the full understanding of nano–bio interfaces is emerging and design principles are beginning to be delineated. Importantly, due to multiple length and time scales ranging from molecular to systemic aspects, a multiscale approach is necessary to seek for a better comprehension of nanomaterials behavior in biological systems. Bridging simulations and experimental research could lead new insight into nanobiotechnology.

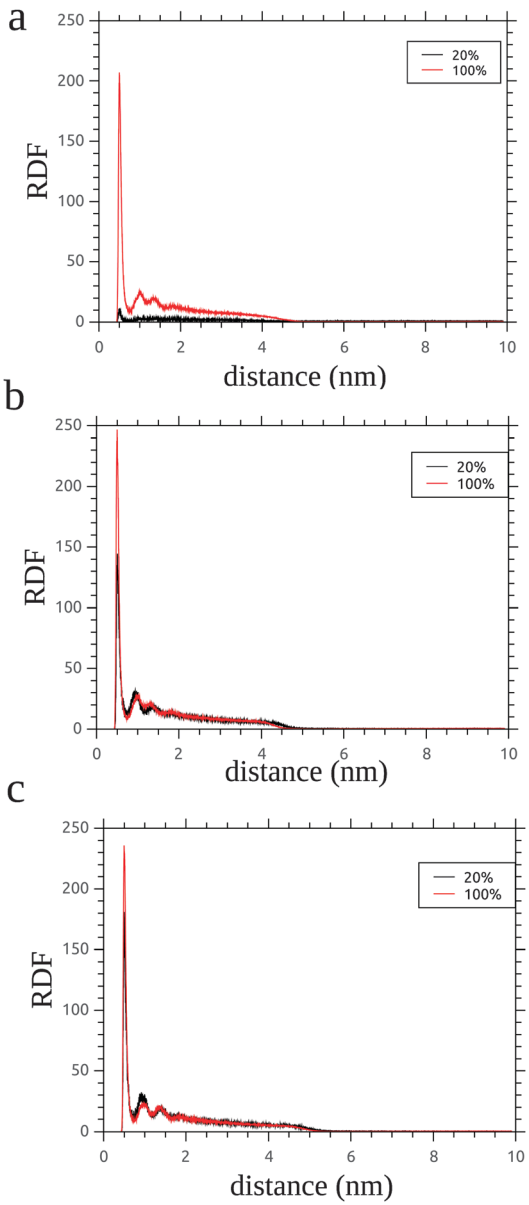

Fig. 6 Radial distribution functions for nanoparticle's cationic terminals and counterions Cl^- employing the ligands (a) 1-octanethiol, (b) 1-dodecanethiol and (c) 1-hexadecanethiol.

5 Conclusions

Molecular dynamics simulations provide a strategy to enable different internalization pathways of nanomaterials through control of surface chemistry. Designing nanoparticles with low charge densities, a mechanism energy-independent of translocation across the membrane might be favored where cationic terminals anchored on the surface of the nanoparticle interact strongly with phosphate groups in both upper and lower membrane leaflets generating a nanoscale pore on the membrane surface. Endocytic pathways might be favored using higher charge densities as evidenced by structural variations of the lipid bilayer. In addition, the simulations suggest an interplay between charge density and ligand length in which shorter ligands and low charge densities more effectively penetrate cell membranes. The simulations highlight molecular details of nanoparticle–membrane interactions and provide design principles to favor different internalization mechanisms by cells.

Acknowledgements

The authors thank the National Council for Scientific and Technological Development (CNPq-Brazil) and Coordination for the Improvement of Higher Level Personnel (CAPES-Brazil) for the financial support.

References

1 D. Peer, J. M. Karp, S. Hong, O. C. Farokhzad, R. Margalit and R. Langer, *Nat. Nanotechnol.*, 2007, **2**, 751–760.
2 G. von Maltzahn, J.-H. Park, K. Y. Lin, N. Singh, C. Schwöppe, R. Mesters, W. E. Berdel, E. Ruoslahti, M. J. Sailor and S. N. Bhatia, *Nat. Mater.*, 2011, **10**, 545–552.
3 T. Dvir, B. P. Timko, D. S. Kohane and R. Langer, *Nat. Nanotechnol.*, 2011, **6**, 13–22.
4 T. Dvir, B. P. Timko, M. D. Brigham, S. R. Naik, S. S. Karajanagi, O. Levy, H. Jin, K. K. Parker, R. Langer and D. S. Kohane, *Nat. Nanotechnol.*, 2011, **6**, 720–725.
5 A. Verma, O. Uzun, Y. Hu, Y. Hu, H.-S. Han, N. Watson, S. Chen, D. J. Irvine and F. Stellacci, *Nat. Mater.*, 2008, **7**, 588–595.
6 T. J. Harris, J. J. Green, P. W. Fung, R. Langer, D. G. Anderson and S. N. Bhatia, *Biomaterials*, 2010, **31**, 998–1006.
7 A. Verma and F. Stellacci, *Small*, 2010, **6**, 12–21.
8 R. A. Petros and J. M. DeSimone, *Nat. Rev. Drug Discovery*, 2010, **9**, 615–627.
9 M. E. Davis, Z. G. Chen and D. M. Shin, *Nat. Rev. Drug Discovery*, 2008, **7**, 771–782.
10 E. Ruoslahti, S. N. Bhatia and M. J. Sailor, *J. Cell Biol.*, 2010, **188**, 759–768.
11 B. Kim, G. Han, B. J. Toley, C.-k. Kim, V. M. Rotello and N. S. Forbes, *Nat. Nanotechnol.*, 2010, **5**, 465–472.
12 H. Lee and R. G. Larson, *J. Phys. Chem. B*, 2006, **110**, 18204–18211.
13 Y. Li and N. Gu, *J. Phys. Chem. B*, 2010, **114**, 2749–2754.
14 H.-m. Ding, W.-d. Tian and Y.-q. Ma, *ACS Nano*, 2012, **6**, 1230–1238.
15 J. P. Prates Ramalho, P. Gkeka and L. Sarkisov, *Langmuir*, 2011, **27**, 3723–3730.
16 K. Yang and Y.-Q. Ma, *Nat. Nanotechnol.*, 2010, **5**, 579–583.
17 S. K. Balasubramanian, J. Jittiwat, J. Manikandan, C.-N. Ong, L. E. Yu and W.-Y. Ong, *Biomaterials*, 2010, **31**, 2034–2042.
18 D. Bechet, P. Couleaud, C. Frochot, M.-L. Viriot, F. Guillemin and M. Barberi-Heyob, *Trends Biotechnol.*, 2008, **26**, 612–621.
19 E. C. Cho, Q. Zhang and Y. Xia, *Nat. Nanotechnol.*, 2011, **6**, 385–391.
20 A. E. Nel, L. Madler, D. Velegol, T. Xia, E. M. V. Hoek, P. Somasundaran, F. Klaessig, V. Castranova and M. Thompson, *Nat. Mater.*, 2009, **8**, 543–557.
21 L.-T. Yan and X. Yu, *ACS Nano*, 2009, **3**, 2171–2176.
22 X. Shi, A. von dem Bussche, R. H. Hurt, A. B. Kane and H. Gao, *Nat. Nanotechnol.*, 2011, **6**, 714–719.
23 J. Lin, H. Zhang, Z. Chen and Y. Zheng, *ACS Nano*, 2010, **4**, 5421–5429.
24 J.-Q. Lin, Y.-G. Zheng, H.-W. Zhang and Z. Chen, *Langmuir*, 2011, **27**, 8323–8332.
25 J. Lee, G. D. Lilly, R. C. Doty, P. Podsiadlo and N. A. Kotov, *Small*, 2009, **5**, 1213–1221.
26 M.-L. Ainalem, R. A. Campbell, S. Khalid, R. J. Gillams, A. R. Rennie and T. Nylander, *J. Phys. Chem. B*, 2010, **114**, 7229–7244.
27 D. Bedrov, G. D. Smith, H. Davande and L. Li, *J. Phys. Chem. B*, 2008, **112**, 2078–2084.
28 E. J. Wallace and M. S. P. Sansom, *Nano Lett.*, 2008, **8**, 2751–2756.
29 H. Chan and P. Kral, *Nanoscale*, 2011, **3**, 1881–1886.
30 K. Lai, B. Wang, Y. Zhang and Y. Zheng, *Phys. Chem. Chem. Phys.*, 2012, DOI: 10.1039/C2CP42027A.
31 Y.-L. Wang, Z.-Y. Lu and A. Laaksonen, *Phys. Chem. Chem. Phys.*, 2012, **14**, 8348–8359.

32 J. Wong-Ekkabut, S. Baoukina, W. Triampo, I.-M. Tang, D. P. Tieleman and L. Monticelli, *Nat. Nanotechnol.*, 2008, **3**, 363–368.
33 E. C. Cho, J. Xie, P. A. Wurm and Y. Xia, *Nano Lett.*, 2009, **9**, 1080–1084.
34 L. Martínez, R. Andrade, E. G. Birgin and J. M. Martínez, *J. Comput. Chem.*, 2009, **30**, 2157–2164.
35 S. Plimpton, *J. Comput. Phys.*, 1995, **117**, 1–19.
36 M. S. Daw and M. I. Baskes, *Phys. Rev. B: Condens. Matter Mater. Phys.*, 1984, **29**, 6443–6453.
37 S. J. Marrink, A. H. de Vries and A. E. Mark, *J. Phys. Chem. B*, 2003, **108**, 750–760.
38 S. J. Marrink, H. J. Risselada, S. Yefimov, D. P. Tieleman and A. H. de Vries, *J. Phys. Chem. B*, 2007, **111**, 7812–7824.
39 S. J. Marrink and A. E. Mark, *J. Am. Chem. Soc.*, 2003, **125**, 15233–15242.
40 S. J. Marrink and A. E. Mark, *J. Am. Chem. Soc.*, 2003, **125**, 11144–11145.
41 M. Louhivuori, H. J. Risselada, E. van der Giessen and S. J. Marrink, *Proc. Natl. Acad. Sci. U. S. A.*, 2010, **107**, 19856–19860.
42 H. J. C. Berendsen, J. P. M. Postma, W. F. van Gunsteren, A. DiNola and J. R. Haak, *J. Chem. Phys.*, 1984, **81**, 3684–3690.
43 U. Essmann, L. Perera, M. L. Berkowitz, T. Darden, H. Lee and L. G. Pedersen, *J. Chem. Phys.*, 1995, **103**, 8577–8593.
44 D. Van Der Spoel, E. Lindahl, B. Hess, G. Groenhof, A. E. Mark and H. J. C. Berendsen, *J. Comput. Chem.*, 2005, **26**, 1701–1718.
45 R. Vácha, F. J. Martinez-Veracoechea and D. Frenkel, *Nano Lett.*, 2011, **11**, 5391–5395.
46 O. Harush-Frenkel, N. Debotton, S. Benita and Y. Altschuler, *Biochem. Biophys. Res. Commun.*, 2007, **353**, 26–32.
47 S. Hong, A. U. Bielinska, A. Mecke, B. Keszler, J. L. Beals, X. Shi, L. Balogh, B. G. Orr, J. R. Baker and M. M. Banaszak Holl, *Bioconjugate Chem.*, 2004, **15**, 774–782.
48 H.-m. Ding and Y.-q. Ma, *Nanoscale*, 2012, **4**, 1116–1122.
49 H. D. Herce and A. E. Garcia, *Proc. Natl. Acad. Sci. U. S. A.*, 2007, **104**, 20805–20810.
50 H.-m. Ding and Y.-q. Ma, *Biomaterials*, 2012, **33**, 5798–5802.
51 Z. Poon, D. Chang, X. Zhao and P. T. Hammond, *ACS Nano*, 2011, **5**, 4284–4292.

